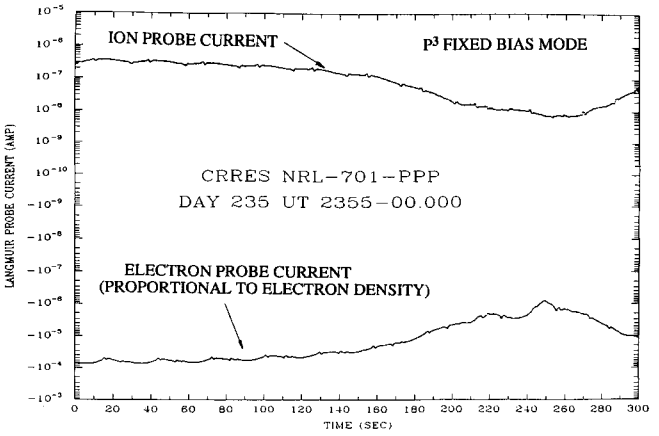

Fig. 3 Measured electron and ion currents near CRRES perigee.

following exception: if both probes have a sweep voltage applied, the bias waveforms must be identical, and in this case, both probes must have the same sweep period. The probe biases are measured with respect to the spacecraft, therefore any variation in spacecraft potential is imposed on the probes.

There are several additional modes of operation which combine pulsed and baseline mode. The first combined mode cycles both probes through four sweep periods of pulsed mode, followed by four sweep periods of baseline mode. The second combined mode cycles the instrument through two sweep periods of pulsed mode, followed by six sweep periods of baseline mode. When the instrument is in baseline mode, measurements from both probes are taken with fixed baseline voltages applied to the probes. There is also a mode in which a given probe can be pulsed between two different baseline voltages, one baseline being in the electron saturation region and the other baseline in the ion saturation region.

The pulsed bias technique has the added advantage of reducing the effects of probe contamination on the measured current. Surface contamination results in unknown probe capacitances which if allowed to fully charge will interrupt current flow to the probe; by pulsing the probe bias, these unknown capacitances do not fully charge within the time resolution of the current measurement. In addition, since the plasma density may be fluctuating during the time of the measurements required to construct the *I-V* curve, saturation current measurements from the fixed baseline are used to correct for current variations on the slope of the *I-V* curve. Correlation with the fixed plasma baseline I-probe, which is sampling ion currents, helps separate plasma density variations from other effects, such as spacecraft wakes and magnetic field anisotropies.

Figure 2 shows a block diagram of the P^3 instrument. Note that there is one sweep voltage generator, with two possible voltage ranges (-3 to $+6$ V and -15 to $+15$ V) and two possible time constants for integration (producing four distinct sweep periods). If the instrument is being operated in pulsed mode, either the sweep voltage or a baseline voltage is multiplexed on the output. Note that the output of the amplifier can be shifted by ± 4 V. Also note that the fundamental difference between the E-probe and the I-probe is that the I-probe is capable of being biased at either the electron saturation current baseline voltage or at the ion saturation current baseline voltage. The instrument can measure currents between $\pm 10^{-10}$ and $\pm 10^{-3}$ A. With a sampling rate of about 6.3 kbps, the instrument spatial resolution depends on the spacecraft velocity and ranges from about 50 m at 350 km altitude (perigee) to approximately 40 m at an altitude of 3000 km.

Initial Measurements

The P^3 experiment was turned on and successfully completed its orbital checkout procedure within weeks after the launch of CRRES on July 25, 1990. All instrument functions are working normally and the instrument was used to provide ionospheric background electron density measurements in support of the first chemical release campaign in September of 1990. An example of the current measurements from both E- and I-probes is shown in Fig. 3, which plots data from a 5-min interval as the spacecraft approaches perigee. For the time period shown, the instrument was in a fixed bias mode in which the E-probe was at a fixed baseline of $+5.5$ V and the I-probe was at a fixed baseline of -2.5 V. Current polarity is included in the plot of Fig. 3, so that the minimum current level on the logarithmic scale is at the midpoint of the vertical axis. Thus, plasma density increases are associated with increases in positive ion current and increases in negative electron current. The relative minimums observed in both probes at about 250 s on the time axis correspond to a decrease in plasma density. The measurement plots also indicate periodic "blips" that appear at periods equal to the spin period of the CRRES spacecraft (about 30 s early in the mission). The spin-modulated currents result from the probes passing through the wake region of the spacecraft, in which relative density decreases occur because the spacecraft is moving at a velocity greater than the thermal ion velocity of the background ionosphere. This effect is observed to varying degrees depending on P^3 instrument modes, and will provide a data base from which to study the structure of the satellite wake.

References

[1]Narcisci, R. S., and Szuszczewicz, E. P., "Direct Measurements of Electron Density, Temperature and Ion Composition in an Equatorial Spread-F Ionosphere," *Journal of Atmospheric and Terrestrial Physics,* Vol. 43, 1981, pp. 463–471.

[2]Szuszczewicz, E. P., Holmes, J. C., Walker, D. N., Rodriguez, P., Swinney, M., and Kegley, L., "An Atlas of Ionospheric F-Region Structures as Determined by the NRL-747/S3-4 Ionospheric Irregularities Satellite Investigation," Naval Research Lab., Rept. 4862, Washington, DC, July 7, 1982.

[3]Rodriguez, P., and Szuszczewicz, E. P., "High-Latitude Irregularities in the Lower F-Region: Intensity and Scale Size Distributions," *Journal of Geophysical Research,* Vol. 89, 1984, pp. 5575–5580.

[4]Rodriguez, P., "An Overview of the LASSII Experiment on CRRES," *Journal of Spacecraft and Rockets,* Vol. 29, No. 4, 1992, pp. 564–565.

[5]Holmes, J. C., and Szuszczewicz, E. P., "Versatile Plasma Probe," *Review of Scientific Instruments,* Vol. 46, 1975, pp. 592–598.

Electron and Proton Wide-Angle Spectrometer (EPAS) on the CRRES Spacecraft

A. Korth,* G. Kremser,† B. Wilken,* W. Güttler‡
Max-Planck-Institut für Aeronomie, D-3411 Katlenburg-Lindau, Germany
S. L. Ullaland§
University of Bergen, Bergen, Norway
and
R. Koga¶
The Aerospace Corporation, Los Angeles, California, 90009

Received May 24, 1991; revision received July 29, 1991; accepted for publication July 29, 1991.

*Senior Scientist.
†Senior Scientist; also Professor of Space Research, Department of Physics, University of Oulu, Oulu, Finland.
‡Senior Engineer.
§Professor, Department of Physics.
¶Member of Technical Staff, Space Sciences Laboratory.

I. Scientific Objectives

ENERGETIC particles are sensitive probes of the global state of the magnetosphere. Complete energy spectra and pitch-angle distributions of energetic particles can be used to identify the mechanisms of access, acceleration, transport, and loss of energetic charged particles in the magnetosphere. Certain unique features of the combined release and radiation effects satellite (CRRES) orbit favor the investigation of these mechanisms on the dayside as well as in the near-Earth tail.

The CRRES orbit provides encounters with the dayside magnetopause during large magnetospheric disturbances and thus enables the study of magnetospheric boundary phenomena. Transport of particles across the magnetopause may arise through wave-particle interactions,[1] steady reconnection,[2] sporadic reconnection,[3] or flux transfer events.[4] Using analytic methods,[5] we intend to monitor themagnetopause position, its orientation, and motion whenever the satellite is in the magnetosphere within a few hundred kilometers of the magnetopause.

The $6.2R_E$ apogee can also provide detailed observations of the substorm development near the equatorial plane. Current substorm models can be examined. Many observations are in agreement with models in which the substorm is triggered in the near-Earth region ($10\text{–}20R_E$) of the plasma sheet by the formation of a neutral line at which magnetic field reconnection suddenly takes place.[6] But there are also observations which show that the substorm may be triggered as close to the Earth as the geosynchronous orbit.[7,8] Roux et al.[8] interpreted these observations in terms of a surface wave generated by a plasma instability in the transition region between more dipolar and more tail-like geomagnetic field lines.

Another aspect is the influence of storm sudden commencements on the particle distribution[9,10] as well as their role in the substorm triggering.[11]

Interactions of particles with waves are important for the coupling of the magnetosphere with the ionosphere. The waves are needed to scatter field-aligned ionospheric particles onto trapped orbits. Conversely, waves act to precipitate particles into the ionosphere. We will examine the effect of different plasma waves on particle precipitation. We will also study the effects of ion-cyclotron waves on protons.

The instrument focuses, furthermore, on studies of the natural radiation environment, their dynamics, and their dependence on the solar activity.

To investigate these processes, high-resolution three-dimensional particle distributions have to be measured. The electron and proton wide-angle spectrometer (EPAS) is well suited for this purpose. It covers the energy range for electrons from 21–285 keV and for protons from 37 ke V–3.2 MeV.

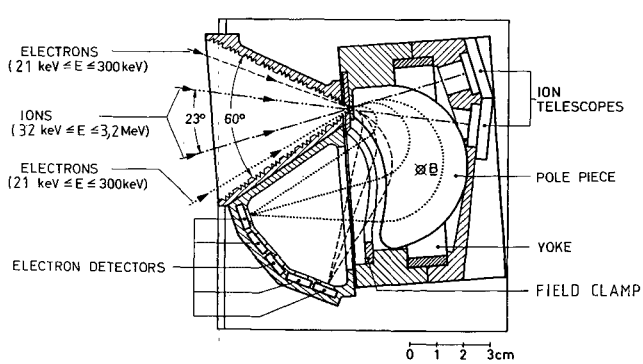

Fig. 1 Schematic drawing of one unit of the spectrometer with a 60-deg opening collimator and an array of five electron detectors and two ion telescopes.

Table 1 EPAS instrument parameters

	Electrons (E0–E9)	Protons (P0–P3)
Energy range	21–300 keV	32–3200 keV
Integral energy channels	>25.5 keV	>32.0 keV
Differential energy channels	1. 21.0–31.5 keV 2. 31.5–40.0 keV 3. 40.0–49.5 keV 4. 49.5–59.0 keV 5. 59.0–69.0 keV 6. 69.0–81.0 keV 7. 81.0–94.5 keV 8. 94.5–112.0 keV 9. 112.0–129.5 keV 10. 129.5–151.0 keV 11. 151.0–177.5 keV 12. 177.5–208.0 keV 13. 208.0–242.5 keV 14. 242.5–285.0 keV	1. 37–54 keV 2. 54–69 keV 3. 69–85 keV 4. 85–113 keV 5. 113–147 keV 6. 147–193 keV 7. 193–254 keV 8. 254–335 keV 9. 335–447 keV 10. 447–602 keV 11. 602–805 keV 12. 805–3200 keV
Look directions of detectors with respect to the spin axis	20 deg (E0); 30 deg (E1) 40 deg (E2); 50 deg (E3) 60 deg (E4); 70 deg (E5) 80 deg (E6); 90 deg (E7) 100 deg (E8); 110 deg (E9)	26 deg (P0) 46 deg (P1) 87 deg (P2) 107 deg (P3)
Angular resolutions in elevation in azimuth	±3 deg ±2 deg	±5 deg ±2 deg
Geometric factor	$\approx 5\times10^{-5}$ cm²sr	2.0×10^{-4} cm²sr
Total weight	4.06 kg	
Total power	2.65 W (average)	

II. Instrument Design

EPAS consists of two identical units to measure electrons simultaneously in ten directions and ions in four directions over a total angular range of ≈110 deg. Each unit contains a magnetic deflection system and an array of solid-state detectors (Fig.1). Particles entering the spectrometer encounter a homogeneous magnetic field of 0.08 T which separates protons and heavier ions from electrons. The magnetic field geometry was designed such that a parallel beam of electrons entering the instrument at a given angle with respect to the axis of the aperture is deflected and focused to a single point irrespective of its energy. The deflection system thus defines a focal curve on which each point corresponds to a given angle of incidence to the spectrometer. Along this focal curve, five rectangular solid-state detectors are mounted which define five angular intervals within the 60-deg aperture of the unit. The focusing can be achieved for electrons with energies between 15 and 300 keV.

The finite width of the entrance hole, the geometry of the pole pieces, and the position of the detectors in the image plane define both the image size of monoenergetic electrons and the angular resolution for the velocity focusing. The angle α (in the elevation direction with respect to the spin axis) is given by the size of the detectors, whereas the angle β (azimuthal direction around the spin axis) is limited by the mechanical aperture to a few degrees (see Table 1) to effectively suppress electron scattering from the pole pieces.

The influence of the fringing magnetic field at the entrance hole and where the electrons exit the sector field can have an important effect on the image aberration. To minimize this effect, a magnetic field clamp is introduced which suppresses the fringing field. The entrance hole has a diameter of 1.2 mm which is approximately the upper limit required by the electron optical properties of the magnet. The transmission of the incident electrons through the magnetic system is a function of the particle energy and the angles of incidence α and β. To

evaluate the focusing properties extensive calibrations were performed (see Sec. IV).

The electrons are detected with rectangular, totally depleted silicon surface barrier detectors. The active area is 5×10 mm^2, and the thickness is 300 μm which is sufficient to absorb electrons with energies up to 300 keV. The Al-side of the detectors is facing the incoming particles. This side is made light tight by using a layer of 120 μg/cm^2 of Al. The total energy range is divided into 14 approximately logarithmically spaced energy channels that are called differential energy channels (see Table 1).

The deflection of ions with energies above 20 keV is negligible. They move on almost straight lines and are detected in solid-state detector telescopes (Fig. 1). For each unit, two telescopes are mounted behind the magnetic deflection system and define two directions for the measurement of ions. Each telescope consists of a front and a back solid-state detector. The front detector has a sensitive area of 50 mm ^{2} and is used for the energy analysis of ions; the back detector (sensitive area of 100 mm^2) provides a veto signal to reject penetrating particles. The front detector of the telescope is operated with the aluminium contact facing the environment. This has two reasons: 1) the Al-contact can be made as thin as 15 μg/cm^2, and 2) the detector lifetime against radiation damage is increased by two or more orders of magnitude in total ion exposure. The energy loss in the dead layer depends on the ion species and its energy. It amounts to about 7–8 keV for protons with an energy of 20 keV. The energy loss is determined at various energies from measurements in the Max-Planck-Institut für Aeronomie (MPAe) ion-accelerator and is included in the energy channels for protons (see Table 1).

The upper energy range of the telescope is defined by the thickness of the front detector, which amounts to 100 μm, and thus covers the energy range up to about 3.2 MeV for protons. The total energy range is divided into 12 approximately logarithmically spaced energy channels.

No identification of the ion species is possible. Since the energy losses in the dead layer increase with Z, we expect a contribution of less than 10% to the count rate of the instrument by ions with $Z \geq 2$ during quiet to moderately disturbed periods. This estimate is based on a comparison of measurements by the electron-proton spectrometer and the ion mass spectrometer on the spacecraft GEOS-1 and -2.

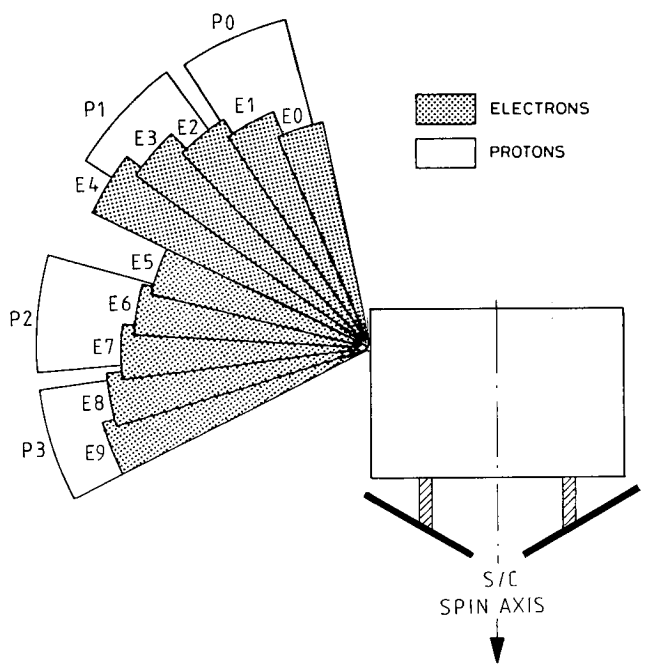

Fig. 2 Look directions of the electron and proton (ion) detectors with respect to the spacecraft spin axis.

Because of the deflection in the magnetic field, electrons with energies below 800 keV cannot reach the proton telescopes. Electrons with higher energies penetrate the front detector, provide a veto signal in the back detector, and are rejected. For this reason, the lowest energy threshold for the protons is essentially given by the noise of the front detector and the analog electronics.

The spectrometer uses $SmCo_5$ as magnetic material. The yoke and the pole pieces are made from magnetically soft iron with a very small coercitive force and high permeability. In order not to disturb magnetic field sensors or other instruments sensitive to magnetic fields on the spacecraft, the magnetic system is completely enclosed by a shielding can of high-permeability material (μ-metal). The shielding factor (ratio of the internal and external field) of such a system is a complicated function of the magnetic permeability, the shape, the size, and the wall thickness. It can only be derived from measurements. A satisfactory attenuation was achieved after a careful annealing process of the soft iron material and after the positioning of the two units in such a way that the magnetic fields between the pole pieces have opposite directions. In this position, the dipole fields cancel each other and only stray fields of higher order will remain. The measured maximum value of the residual field was 2 nT at a distance of 50 cm from the center of the sensor system.

The sensor is thermally isolated from the analog electronics, since the detectors have to be operated at a lower temperature than the electronics. In fact, the detector noise can be substantially reduced if the detectors are operated at temperatures between -20°C and $+5$°C. Therefore the front of the sensor which is facing the outside environment is designed as a radiator. Small electrically conducting second surface mirrors are fixed to the sensor to radiate the heat into space. From measurements during the solar simulation tests we expect sufficiently low sensor temperatures.

The EPAS spectrometer contains two of the described units and covers in total an angular range of ≈ 110 deg. The sensor is mounted on the platform of the spacecraft and is directed such that the angular range of 110 deg is located in the meridian plane of the satellite. The spectrometer is able to detect electrons simultaneously from ten directions and protons from four directions (Fig. 2). The spin axis of the CRRES spacecraft is located in the orbital plane.

The three-dimensional directional distribution can be converted into a pitch-angle distribution with the help of the magnetic field measurements on the same satellite. The pitch angle is a function of the local magnetic field vector with respect to the spin axis and the look directions of the different detectors.

III. Analog Electronics

The analog electronics box is mechanically connected to the sensor box, but electrically and thermally isolated from it. The analog box consists of many individual housings to achieve a careful shielding between the amplifier chains and thus to avoid cross talk. The electrical interface between the analog box and the data processing unit (DPU) only allows the transmission of digital pulses.

The functional block diagram of the analog electronics of the EPAS instrument is shown in Fig. 3. All solid state detectors (protons: P0–P3; electrons: E0–E9) are followed by charge-sensitive preamplifiers, pulse amplifiers, pulse formers, and discriminators.

The ion telescopes produce three different sets of data: the count rates of the front detectors (P0–P3), the count rates of the back detectors (U0–U3), and coincidence counts of the front and back detectors. The count rates of the front detectors go to a "Proton Selector" unit that selects one out of the four detectors for energy analysis in the proton pulse-height analyzer (PHA). This analysis is only carried out if a coincidence between front and back detectors has not occurred. These data are called differential count rates. The energy thresholds are given in Table 1. Simultaneously the count rates

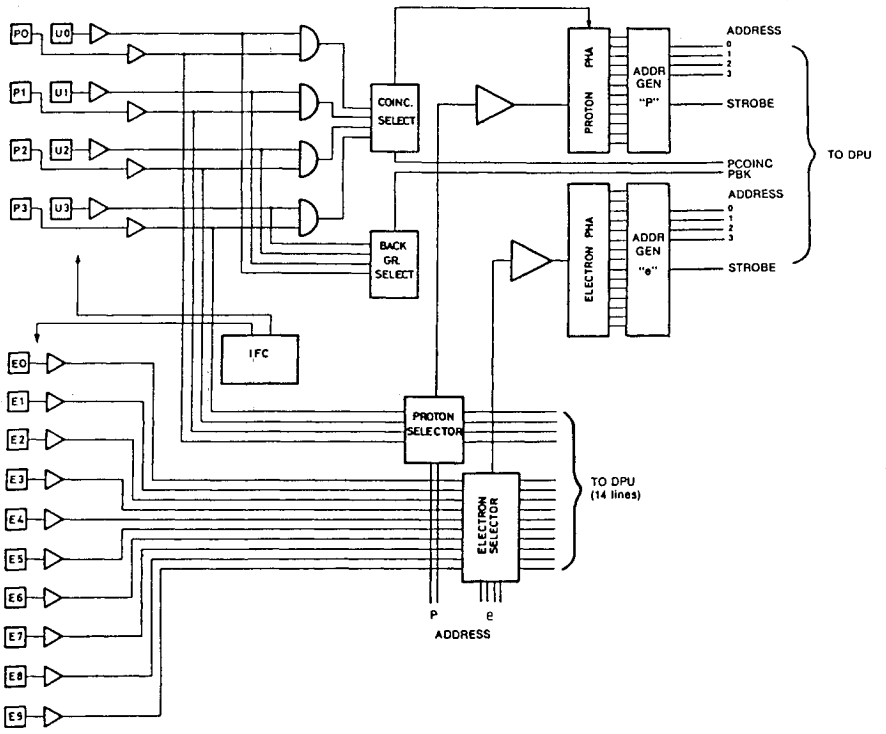

Fig. 3 Block diagram of the analog electronics.

of the four front detectors are routed via discriminators to the DPU; these are called integral count rates. The energy thresholds are given in Table 1.

The data lines from the ten electron detectors (E0–E9) pass the "Electron Selector" that determines on which of the ten channels energy analysis is carried out in the electron PHA. The ten data lines are also routed via discriminators as integral count rates directly to the DPU.

The proton and electron PHAs sort the count rates from one selected proton and from one electron detector into 12 or 14 different energy intervals, respectively. The differential count rates are taken consecutively from the various electron and proton detectors. The sampling time for the protons amounts to 512 ms and for the electrons to 256 ms. During the normal mode, the proton detector sequence is P2, P0, P1, P3, P2, P0; P2, . . .; and the electron detector sequence is E6, E9, E2, E7, E4, E0, E6, E8, E1, E5, E3, E0; E6, . . . These sequences can be changed by command.

The integral count rates are obtained simultaneously for all detectors. The time resolution for the integral count rates of electrons and protons amounts to 512 ms.

An in-flight test generator (IFC) is used to control the operation of the instrument. Pulses with varying amplitudes are fed into the inputs of the charge-sensitive amplifiers and are counted at the outputs of the two PHAs as well as at the outputs of the discriminators. The in-flight calibrator is initiated via the IFC ON line and controlled by the frequency of the IFC clock.

The DPU provides 16 scalers to monitor the integral counting rates from the ten electron detectors, four proton front detectors, and coincidence and back detector counting rates of the proton detector selected for pulse-height analysis. Two scalers in the DPU are driven by two sets of 4-bit address and single strobe lines, one each for the proton and electron detector selected for pulse-height analysis. The DPU contains power supplies to provide power to the sensor with various voltages. Details of the DPU are published in this volume.[12]

IV. Instrument Calibration with an Electron Beam

In general, the transmission of incident electrons through the magnetic system shown in Fig. 1 is a function of particle energy and the incidence angles α and β. The detection efficiency depends on the active area and relevant parameters of the detector.

To evaluate the focusing properties quantitatively and therewith the transmission efficiency, the complete system was calibrated with electrons in the energy range of $20 \leq E \leq 150$ keV supplied by an electrostatic accelerator and in the energy range of $70 \leq E \leq 400$ keV using electrons from a Van-de-Graaf generator. (Both the accelerator and the generator are facilities of the Goddard Space Center, Greenbelt, Maryland.) The experiment was mounted on a platform allowing rotations around two axes perpendicular to each other to define the angles of incidence α and β. The accuracy for both angles was 0.1 deg. The alignment of the experiment in the vacuum chamber with respect to the center of the beam line was achieved by optical autocollimation. The beam diameter was 15 mm, which is much larger than the aperture diameter of 1.2 mm. A monitor detector was mounted on a mechanical device and could be moved directly in front of the collimator. The aperture diameter of the monitor detector was 2.0 mm. The response of the monitor detector was used to inspect the spectral shape of the beam and to normalize the response of the magnetic system.

The signals generated in the five electron detectors were processed with individual amplifier-discriminator-counter chains allowing simultaneous measurements from all detectors. A PHA was used to take spectra routinely from each detector in order to detect spectral distortions due to scattering in the instrument.

The counting rates from detectors E0–E9 and the monitor detector were used to determine the transmission efficiency. The spectral information was used to correct scattering effects and system noise.

For the flight data analysis, we will use from the calibration measurements two two-dimensional tables which give 1) actual look directions for all electron detectors vs energy channels and 2) geometric factors for all electron detectors vs energy channels. Average values are given in Table 1.

V. Performance After Launch

The EPAS instrument on CRRES has been operating successfully since launch. The instrument design temperatures were achieved. The operating temperatures reached -20°C

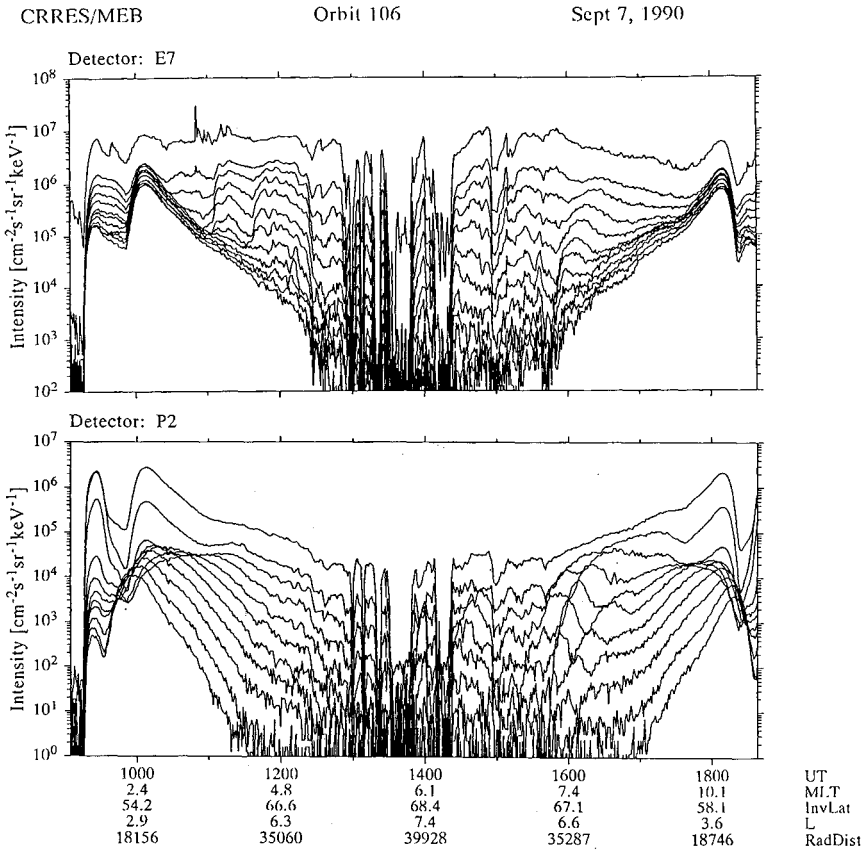

Fig. 4 Differential electron intensities in 12 energy channels from detector E7 and ion intensities in ten energy channels from detector P2 during CRRES orbit 106.

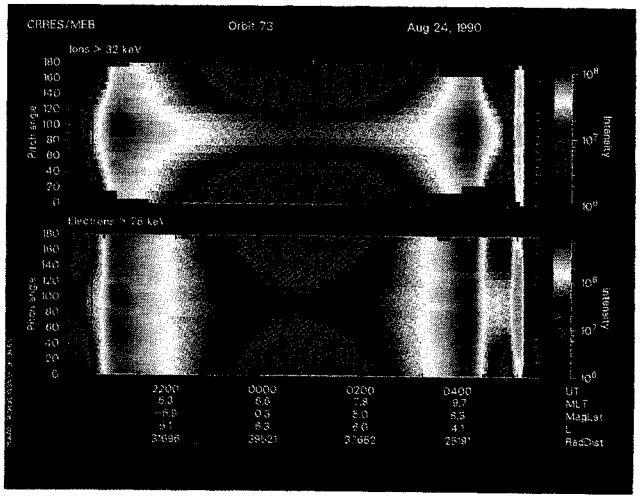

Fig. 5 Integral electron intensities ($E > 25.5$ keV) and proton intensities ($E > 32$ keV) in a time vs pitch-angle diagram from CRRES orbit 73.

for the sensor and +6°C for the analog electronics. The detector noise levels were comparable to the values measured on ground.

Fig. 4 displays the intensities measured in 12 differential energy channels of the electron detector E7 and ten differential energy channels of the proton detector P2 during the CRRES orbit 106. The data were averaged over 1 min. The lowest energy channel is displayed on top of each panel and is given as first channel in Table 1. Near $L = 6$ several dropout events were observed. During these events the count rates dropped to zero and the detector noise level could be determined, especially for the lowest differential electron and proton channels.

A second example of the instrument performance is shown in Fig. 5. The integral electron ($E > 25.5$ keV) and ion ($E > 32$ keV) intensities are displayed in a time vs pitch-angle diagram. The data were obtained during orbit 73 and were averaged over 1 min. The intensity is given in a color coded logarithmic scale. During this orbit the magnetosphere was not disturbed. The inner and outer radiation belts together with the slot region are clearly identified.

Acknowledgments

The MEB spectrometer was designed and constructed with support from the Max-Planck Gesellschaft zur Förderung der Wissenschaften. Grants were received from the United States Air Force under AFOSR-85-0237 and from the Norwegian Research Council for Science and the Humanities to the University of Bergen. The data processing unit and instrument integration were supported at The Aerospace Corporation under Air Force Space Systems Division Contract F04701-88-C-0089.

References

[1]Eviatar, A., and Wolf, R. A., "Transfer Processes at the Magnetopause," *Journal of Geophysical Research*, Vol. 73, No. 17, 1968, p. 5561-5576.

[2]Korth, A., Kremser, G., and Daly, P. W., "Observations of Field-Aligned Energetic Electron and Ion Distributions Near the Magnetopause at Geosynchronous Orbit," *Journal of Geophysical Research*, Vol. 87, No. A12, 1982, pp. 10,413-10,419.

[3]Paschmann, G., et al., "Plasma Acceleration at the Earth's Magnetopause: Evidence for Reconnection," *Nature*, Vol. 282, Nov. 1979, pp. 243-246.

[4]Russell, C. T., and Elphic, R. C., "Initial ISEE Magnetometer Results: Magnetopause Observations," *Space Science Reviews*, Vol. 22, No. 6, 1978, pp. 681-715.

[5]Williams, D. J., Fritz, T. A., Wilken, B., and Keppler, E., "An Energetic Particle Perspective of the Magnetopause," *Journal of Geophysical Research*, Vol. 84, No. A11, 1979, pp. 6385-6396.

[6]Baker, D. N., Akasofu, S.-I., Baumjohann, W., Bieber, J. W., Fairfield, D. H., Hones, E. W., Jr., Mauk, B., McPherron, R. L., and Moore, T. E., "Substorms in the Magnetosphere, Solar Terrestrial Physics: Present and Future," *NASA Ref. Publ.*, pp. 1120-1128, Chap. 8, 1984.

[7]Kremser, G., Korth, A., Ullaland, S. L., Perraut, S., Roux, A., Pedersen, A., Schmidt, R., and Tanskanen, P., "Field-Aligned Beams of Energetic Electrons (16 keV $\leq E \leq$80 keV) Observed at Geosynchronous Orbit at Substorm Onsets," *Journal of Geophysical Research*, Vol. 93, No. A12, 1988, pp. 14,453-14,464.

[8]Roux, A., Perraut, S., Robert, P., Morane, A., Pedersen, A., Korth, A., Kremser, G., Aparicio, B., Rodgers, D., and Pellinen, R., "Plasmasheet Instability Related to the Westward Travelling Surge," *Journal of Geophysical Research*, Vol. 96, No. A10, 1991, pp. 17,697-17,714.

[9]Korth, A., Kremser, G., Cornilleau-Wehrlin, N., and Solomon, J., "Observations of Energetic Electrons and VLF Waves at Geostationary Orbit During Storm Sudden Commencements (SSC)," *Solar Wind-Magnetosphere Coupling*, edited by Y. Kamide and J. A. Slavin, Terra Scientific Publishing Co., Tokyo, Japan, 1986, pp. 391-399.

[10]Wilken, B., Baker, D. N., Higbie, P. R., Fritz, T. A., Olsen, W. P., and Pfitzer, K. A., "Magnetospheric Configuration and Energetic Particle Effects Associated with a SSC: A Case Study of the CDAW 6 Event on March 22, 1979," *Journal of Geophysical Research*, Vol. 91, No. A2, 1986, pp. 1459-1473.

[11]Ullaland, S. L., Kremser, G., Tanskanen, P., Korth, A., Torkar, K., Block, L., and Iversen, I. B., "Influence of a Storm Sudden Commencement on the Development of a Magnetospheric Substorm: Ground, Balloon, and Satellite Observations," *Journal of Geophysical Research*, (submitted for publication), 1992.

[12]Koga, R., Imamoto, S. S., Katz, N., Pinkerton, S. D., "Data Processing Units for Eight Magnetospheric Particle and Field Sensors," *Journal of Spacecraft and Rockets*, Vol. 29, No. 4, 1992, pp. 574-579.

CRRES Spectrometer for Electrons and Protons

R. W. Nightingale,* R. R. Vondrak,† E. E. Gaines,* W. L. Imhof,‡ R. M. Robinson,§ S. J. Battel,¶ D. A. Simpson,** and J. B. Reagan††
Lockheed Palo Alto Research Laboratory, Palo Alto, California 94304

Introduction

IMPORTANT components of the magnetospheric plasma to be explored by the CRRES are the energetic electrons and protons that populate the Earth's radiation belts. The fluxes of these particles depend critically on the production and loss mechanisms in the radiation belts and exhibit dynamic behavior in response to solar and geomagnetic activity.[1,2] The understanding of these processes requires detailed measurements of the particle distribution functions including the pitch angle. Previous measurements of energetic electrons and protons have been made by instruments on satellites such as Ogo 5,[3] SCATHA,[4] (S/C) 1979-053, and (S/C) 1982-019,[1,2] but the unique CRRES orbit offers exciting new possibilities for developing improved models of the inner and outer radiation belts.[5,6] For example, the particle distributions measured along the spacecraft trajectory can be used to map the two-dimensional radiation belt morphology in the orbit plane for $1.05 < L \leq 7$ near the geomagnetic equator.

The ONR 307-3 Spectrometer for Electrons and Protons (SEP) is one component of the ONR 307 Energetic Particles and Ion Composition experiment. SEP measures the energy and pitch angle distributions of energetic electrons and protons throughout the CRRES orbit. The specific science objectives of the SEP experiment are 1) to understand the physics of the sources, losses, energization, transport, and lifetimes of energetic particles in the Earth's radiation belts; 2) to understand the details of wave-particle interactions (WPI), both natural and man made, that result in precipitation of radiation belt particles; and 3) to utilize this experimental data base to greatly improve the accuracy of trapped radiation belt models.

Experiment Description and Operations

The SEP design is based heavily on the successful SC-3 spectrometer[4,7] flown on the SCATHA mission. Unlike the single-detector system used on SCATHA, SEP consists of three solid-state particle spectrometers oriented at 40, 60, and 80 deg from the spacecraft spin axis. A cross-sectional view of one of the telescopes is shown in Fig. 1. Each spectrometer has four detector elements labeled A, D, E, and E′. Various logic combinations of the four detector elements in each spectrometer are used to determine the particle types and energy ranges, which are measured sequentially. The operational modes of each telescope are individually commandable.

The D detector, which is 200-μm-thick intrinsic silicon, is used to measure both the rate of energy loss of the higher-energy particles and to directly stop and measure the low-energy particles. The E detector, which consists of a stack of five 2-mm-thick silicon surface-barrier detectors in parallel, is located behind the D detector to stop the higher-energy particles and to measure their total energy loss. The E′ detector, which is a 1000-μm-thick piece of silicon, is located behind the E detector and is used as an active collimator. Following it is a tungsten absorber that sets the upper energy limit for analysis. The entire telescope-configured stack is surrounded by the anticoincidence A detector, which consists of a plastic scintillator viewed by a photomultiplier tube. The A detector senses and rejects energetic particles and bremsstrahlung that penetrate either the outer shielding walls of aluminum and tungsten or the silicon detector stack and tungsten absorber. The detector stack is located behind a long, narrow collimator that defines the 3-deg angular field of view full width at half maximum (FWHM). The aluminum and tungsten effectively stop electrons with energy up to 5 MeV and bremsstrahlung photons with energy up to about 150 keV.

Each of the three identical SEP particle telescopes has a high-resolution, 3-deg (FWHM) field of view provided by a long collimator (20 cm) containing 10 baffles. The collimators are identical to the ones used on the SC-3 instrument,[4] providing an instrument geometric factor of $\sim 3 \times 10^{-3}$ cm^2-sr. For the 80- and 60-deg telescopes, measurements over 12 energy channels are obtained every 0.25 s with a dead time of 2 ms. Because of telemetry restrictions, the 40-deg telescope accumulates for 0.5 s with a dead time of 4 ms.

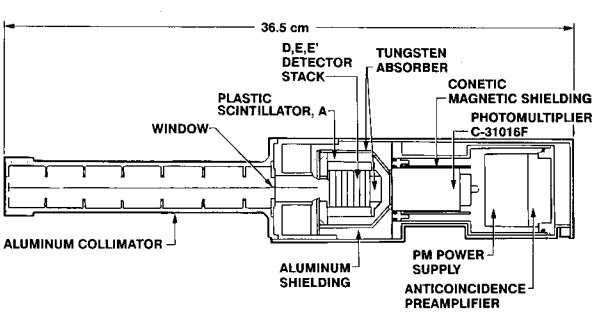

Fig. 1 Cross-sectional view of one of the SEP telescopes.

Received June 18, 1991; revision received Sept. 3, 1991; accepted for publication Sept. 3, 1991.

*Research Scientist.
†Manager. Associate Fellow AIAA.
‡Consulting Scientist.
§Staff Scientist.
¶Consultant, Battel Engineering. Member AIAA.
**Senior Staff Research Engineer.
††General Manager. Fellow AIAA.